



Novel organogel harnessing Excited-State Intramolecular Proton Transfer process with aggregation induced emission and photochromism



Miao Luo^a, Sheng Wang^{a,*,**}, Meiling Wang^a, Shaorong Huang^a, Chengpeng Li^a,
Lin Chen^b, Xiang Ma^{b,*}

^a College of Basic Education, School of Chemistry and Chemical Engineering, Lingnan Normal University, Zhanjiang, 524037, Guangdong, PR China

^b Key Laboratory for Advanced Materials and Institute of Fine Chemicals, East China University of Science and Technology, Meilong Road 130, Shanghai, 200237, PR China

ARTICLE INFO

Article history:

Received 31 March 2016

Received in revised form

21 April 2016

Accepted 22 April 2016

Available online 25 April 2016

Keywords:

Aggregation-induced emission

Tetraphenylethylene derivatives

Organogelator

Salicylideneaniline

Photochromism

ABSTRACT

Two novel aggregation-induced emission compounds harnessing Excited-State Intramolecular Proton Transfer process based on salicylideneaniline derived from tetraphenylethylene and cholesterol moieties were synthesized and characterized. One of the compounds could gelate in cyclohexane exhibiting gelation-induced enhanced emission and the emission intensities can be reversibly changed with the gel-solution transition by alternate cooling and heating. Moreover, this compound showed photochromic behavior both in gel and solid states under UV light irradiation due to the loose packing of the molecules and permitting the molecule to rotate, which may be a potential candidate for external stimuli-responsive materials through tuning the self-assembly process of the functional gelator.

© 2016 Elsevier Ltd. All rights reserved.

1. Introduction

Low-molecular mass organogelators (LMOGs) have received immense interest in supramolecular chemistry and materials science due to their potential applications in sensors, cosmetics, catalysis, energy harvesting, drug delivery systems, switches and other related fields [1–9]. LMOGs consisting of low molecular weight molecules can self-assemble into various nanostructures, such as fibers, rods, ribbons and other aggregates, through multiple noncovalent interactions [10–13], to form entangled three-dimensional networks preventing the solvent molecules from flowing [14–16]. Most LMOGs possessing stimulus-responsive properties show reversible changes in morphology and/or physical properties in response to various external stimuli such as pH,

temperature, light, sound, and shearing stress, thus potentially applicable in sensors, switches, chemical valves and drug delivery systems [7,14,17–20].

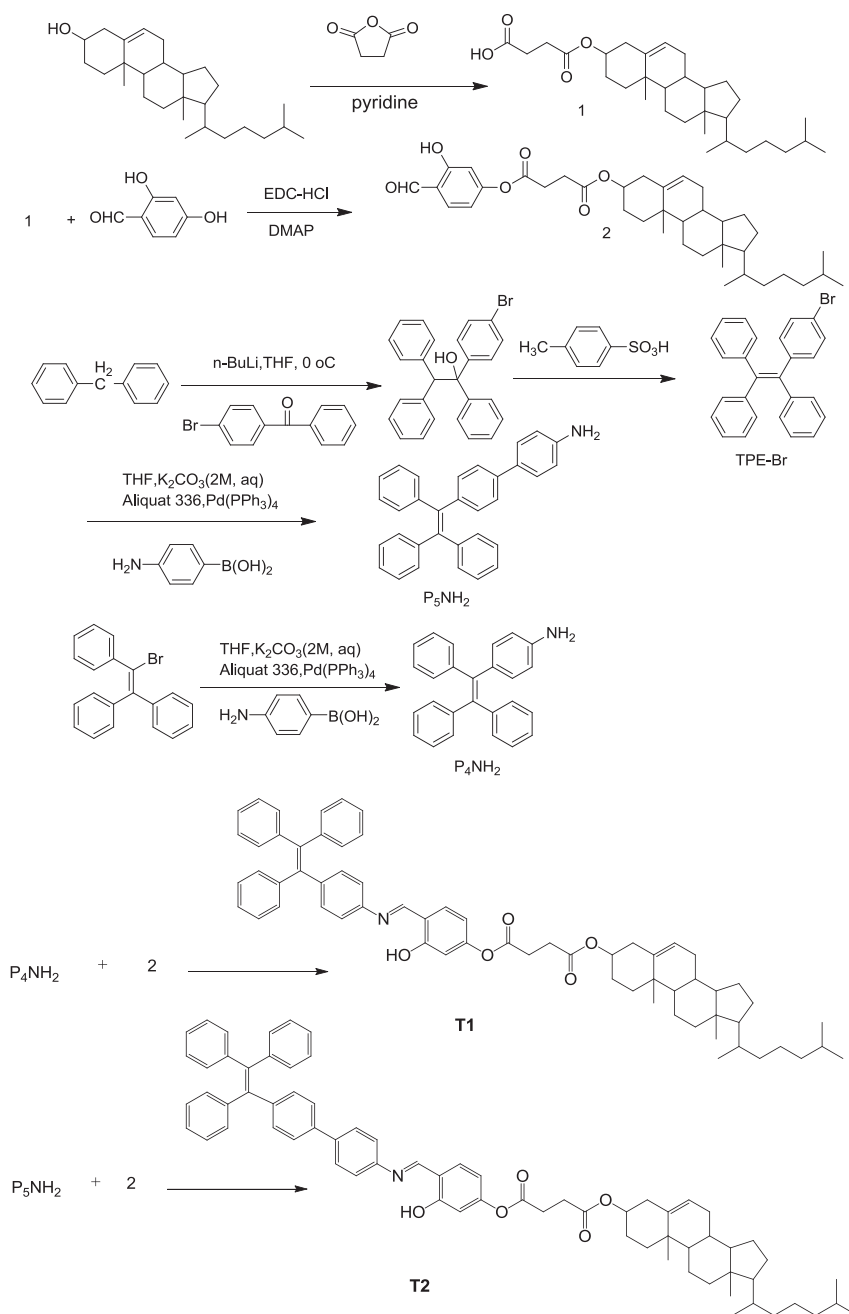
Nowadays, a lot of attentions have been paid on organic fluorescent molecules harnessing the ESIPT process, which show unique photophysical properties and have potential applications in chemical sensors, proton transfer lasers, fluorescence imaging, and organic light-emitting diodes (OLEDs) [21]. However, most of chromophores harnessing the ESIPT process suffer from aggregation caused quenching and thus limited their practical applications. Fortunately, a novel phenomenon of aggregation-induced emission (AIE) was first found by Tang's group in 2001 [22–24]. Then more and more significant progress has been made via the AIE mechanism and AIE-active molecules. Several ESIPT molecules possessing AIE characteristics have been recently reported [2,25–32]. However, the number of organogelator harnessing ESIPT process is still very limited so far, and LMOGs based on salicylideneaniline derived from tetraphenylethylene (TPE) and cholesterol moieties have not been reported to the best of our knowledge.

Herein, we report two novel AIE compounds (**T1** and **T2**, Scheme 1) by introducing tetraphenylethylene and cholesterol moieties

* Corresponding author. Key Laboratory for Advanced Materials and Institute of Fine Chemicals, East China University of Science and Technology, Shanghai, 200237, PR China.

** Corresponding author. College of Chemistry Science & Technology, Lingnan Normal University, Zhanjiang, 524048, PR China.

E-mail addresses: dyesws@126.com (S. Wang), maxiang@ecust.edu.cn (X. Ma).



Scheme 1. Synthetic routes for T1 and T2.

into salicylideneaniline system. TPE, a propeller-like luminogen, as a prototypical AIEgen has been under intensive and extensive investigations [33–36]. Cholesterol is favorable for facilitating gelation of solvents and thus been widely used for designing new LMOGs [1,11]. Moreover, a Schiff base bearing an *o*-hydroxyl group on the benzene ring is responsible for ESIPT process [25]. The self-assembly, ESIPT process and photochromism properties are also elucidated.

2. Experimental

2.1. Materials and instruments

4-Aminophenylboronic acid, 4-bromophenyl

phenylmethanone, 2-bromo-1,1,2-triphenylethylene, diphenylmethane, cholesterol, succinic anhydride, 2,4-dihydroxybenzaldehyde, *n*-butyl lithium, aliquat 336, tetrakis (triphenylphosphine) palladium (0) were purchased from Aladdin company and used as received. 4-dimethylaminopyridine (DMAP), 4-toluene sulfonic acid, 1-(3-dimethylaminopropyl)-3-ethylcarbodiimide hydrochloride (EDC-HCl) were purchased from Shanghai Darui company (China) used as received. Ultra-pure water was used in the experiments. Tetrahydrofuran (THF) was distilled from sodium/benzophenone. All other reagents and solvents were purchased as analytical grade from Zhangjiang Kangbai Company (China) and used without further purification. 1-bromo-4-(1,2,2-triphenylvinyl)benzene (TPE-Br) [37,38], 4-(1,2,2-triphenylvinyl)benzene-amine (P₄NH₂) [7] and 4'-(1,2,2-

triphenylvinyl)biphenyl-4-amine (P₅NH₂) [7] were prepared according to the literature methods.

The IR spectra were measured on a Nicolet-6700 FT-IR spectrometer by incorporating the samples in KBr disks. Proton and carbon nuclear magnetic resonance (¹H NMR and ¹³C NMR) spectra were measured on a Bruker AVANCE III spectrometer [CDCl₃, tetramethylsilane (TMS) as the internal standard]. The electronic spray ionization (ESI) high-resolution mass spectra were tested on a HP 5958 mass spectrometer. The SEM images were obtained using a Hitachi S-4800 spectrometer. The CD spectra were recorded on JASCO J-815 CD spectropolarimeter. The UV/Vis spectra were determined on a Shimadzu-2550 spectrophotometer and a Shimadzu-3600 spectrophotometer. Photoluminescence spectra (PL) were measured on a Cary Eclipse spectrometer with 10 nm and 10 nm slit widths for excitation and emission, respectively.

2.2. Synthesis of 3-cholesteryloxycarbonylpropanoic acid (**1**)

A solution of cholesterol (5.80 g, 15 mmol), succinic anhydride (1.50 g, 15 mmol), pyridine (1.00 mL), and dry heptane (150 mL) were heated to reflux for 21 h and cooled to room temperature. The resulting precipitate was recrystallized twice from acetone. Yield: 70%.

2.3. Synthesis of compound 2-Hydroxy-4-(3-cholesteryloxycarbonylpropionyloxy) benzaldehyde (**2**) [3]

Compound **1** (2.50 g, 5.1 mmol) and 2,4-dihydroxybenzaldehyde (0.9 g, 6.5 mmol) were dissolved in dry CH₂Cl₂ (50 mL) containing pyridine (1.8 mL). The solution was cooled to 0–5 °C and a small amount of DMAP and EDC-HCl (2.50 g, 10 mmol) were added. The mixture was stirred for 4 h at 0–5 °C and left for 24 h at room temperature. A white precipitate was removed by filtration. After the solvent was evaporated under reduced pressure, the resultant residue was purified by column chromatography on silica gel (cyclohexane/ethyl acetate 5:1). Yield: 20%; IR (KBr): $\nu = 3436\text{ cm}^{-1}$ (hydroxy), 1765 and 1730 cm^{-1} (ester carbonyl), 1659 cm^{-1} (aldehyde carbonyl); ¹H NMR (400 MHz) δ 11.22 (s, 1H), 9.86 (s, 1H), 7.57 (d, $J = 8.4\text{ Hz}$, 1H), 6.83–6.76 (m, 2H), 5.38 (d, $J = 3.8\text{ Hz}$, 1H), 4.66 (m, 1H), 2.88 (t, $J = 6.7\text{ Hz}$, 2H), 2.72 (t, $J = 6.6\text{ Hz}$, 2H), 2.33 (d, $J = 7.8\text{ Hz}$, 2H), 2.06–1.78 (m, 6H), 1.40–1.23 (m, 7H), 1.12 (m, 7H), 1.04–0.85 (m, 17H), 0.67 (s, 3H).

2.4. Synthesis of **T1**

A solution of **2** (0.1500 g, 0.24 mmol) and P₄NH₂ (0.0859 g, 0.24 mmol) in ethanol (50 mL) was heated to reflux for 12 h and cooled to room temperature. The precipitate formed was collected by filtration and washed by alcohol for 3 times to get **T1** as light yellow solid. Yield: 78.9%; m.p 178.0–180.0 °C; IR (KBr): $\nu = 3425\text{ cm}^{-1}$ (hydroxy), 1763 and 1730 cm^{-1} (ester carbonyl), 1622 cm^{-1} (C=N); ¹H NMR (400 MHz, CDCl₃) δ 8.61 (s, 1H), 7.42 (d, $J = 8.4\text{ Hz}$, 1H), 7.22–7.01 (m, 21H), 6.90 (d, $J = 1.8\text{ Hz}$, 1H), 6.73 (dd, $J = 8.4, 1.9\text{ Hz}$, 1H), 5.40 (d, $J = 4.2\text{ Hz}$, 1H), 4.68 (m, 1H), 2.89 (t, $J = 6.6\text{ Hz}$, 2H), 2.74 (t, $J = 6.6\text{ Hz}$, 2H), 2.38–2.32 (m, 2H), 2.07–1.81 (m, 6H), 1.40–0.86 (m, 31H), 0.70 (s, 3H); ¹³C NMR (CDCl₃, 75 MHz) δ (ppm): 171.5, 170.5, 164.0, 161.0, 143.6, 143.5, 139.5, 132.5, 131.4, 131.3, 126.6, 122.8, 120.5, 110.4, 71.6, 56.8, 56.1, 50.1, 42.3, 39.9, 39.6, 37.9, 36.9, 36.7, 36.1, 35.7, 31.8, 29.6, 28.3, 28.2, 27.8, 24.4, 23.7, 22.9, 22.7, 21.2, 21.2, 19.4, 18.7, 11.9; MALDI-TOF MS (ES+): m/z 936.55 ([M]⁺, calcd for C₆₄H₇₃NO₅, 936.55).

2.5. Synthesis of **T2**

A solution of **2** (0.2190 g, 0.36 mmol) and P₅NH₂ (0.0859 g,

0.36 mmol) in ethanol (50 mL) was heated to reflux for 12 h and cooled to room temperature. The precipitate formed was collected by filtration and washed by alcohol for 3 times to get **T2** as light yellow solid. Yield: 86.5%; m.p 228.0–230.0 °C; IR (KBr): $\nu = 3442\text{ cm}^{-1}$ (hydroxy), 1764 and 1733 cm^{-1} (ester carbonyl), 1621 cm^{-1} (C=N); ¹H NMR (400 MHz, CDCl₃) δ 8.68 (s, 1H), 7.64 (d, $J = 7.8\text{ Hz}$, 2H), 7.47–7.33 (m, 5H), 7.21–7.05 (m, 19H), 6.84 (s, 1H), 6.76 (d, $J = 7.5\text{ Hz}$, 1H), 5.41 (d, $J = 4.1\text{ Hz}$, 1H), 4.69 (m, 1H), 2.91 (t, $J = 6.6\text{ Hz}$, 2H), 2.75 (t, $J = 6.6\text{ Hz}$, 2H), 2.36 (d, $J = 7.6\text{ Hz}$, 2H), 2.08–1.82 (m, 6H), 1.41–1.26 (m, 7H), 1.22–1.08 (m, 7H), 1.07–0.86 (m, 17H), 0.70 (s, 3H); ¹³C NMR (CDCl₃, 75 MHz) δ (ppm): 171.4, 170.6, 147.0, 143.8, 143.1, 141.3, 140.4, 139.6, 137.8, 134.9, 133.1, 131.9, 131.4, 127.7, 127.6, 126.5, 126.0, 122.8, 121.6, 113.9, 110.6, 74.6, 56.7, 56.1, 50.0, 42.3, 39.7, 39.6, 38.0, 36.8, 36.3, 35.9, 32.0, 29.5, 27.6, 24.4, 23.8, 22.8, 22.4, 21.0, 19.3, 18.9, 12.2; MALDI-TOF MS (ES+): m/z 1012.58 ([M]⁺, calcd for C₇₀H₇₇NO₅, 1012.58).

3. Result and discussion

3.1. Synthesis

The target compounds were synthesized according to the routes depicted in Scheme 1. The molecular structure of the target compounds consisted of three parts: the tetraphenylethylene, the salicylaldehyde and the cholesterol moieties. The design strategy of the salicylaldehyde molecule, including a hydrogen bonding site and a fluorescent tetraphenylethylene core, is expected to make the molecule display photochromism. One of the major objectives of this study is to examine the influence of the linker on the properties of the compounds. Their molecular structures were confirmed by ¹H and ¹³C NMR spectroscopy, mass spectrometry, and Fourier-transform infrared spectroscopy.

3.2. Gelation properties

The gelation behavior of compounds **T1** and **T2** were tested in different solvents, with 3.0% (w/v) as a standard concentration. The results are summarized in Table 1. It can be found that a small difference of molecule structure greatly affected the gelation ability. For **T2**, there is one more phenyl unit than **T1** between the link of TPE and *o*-hydroxyl benzene unit. Surprisingly, **T1** could not form stable organogels in any organic solvents, while **T2** could only gelate in cyclohexane with critical gelator concentrations (CGC) about 20 mg/mL by using the ‘stable to inversion of a test tube’ method [30,39] and the gel-to-sol phase transition temperature (T_{gel}) about 68 °C by using ‘the ball dropping method’ [18].

To investigate the aggregation morphology of the organogel, xerogel of **T2** prepared by slow evaporation of cyclohexane from the corresponding organogel, was studied by field emission scanning electron microscopy (FE-SEM). As shown in Fig. 1, the xerogel of **T2** was composed of fibrous structure about 100 nm in width and

Table 1
Gelation properties of **T1** and **T2** in various solvents.

Solvents	T1	T2	Solvents	T1	T2
Cyclohexane	S	G	Toluene	S	S
DMF	P	S	Butyl alcohol	P	I
DMSO	S	S	<i>p</i> -Xylene	S	S
1-Octanol	P	I	Petroleum ether	I	I
1,4-Dioxane	S	S	Ethanol	I	I
Ethylene glycol	I	I	THF	S	S
Ethyl acetate	S	S	Dichloromethane	S	S
Acetone	I	I	Acetonitrile	I	I
Diethyl ether	S	I	Methyl alcohol	I	I

G: stable gel formed at room temperature; S: soluble; I: insoluble; P: precipitate.

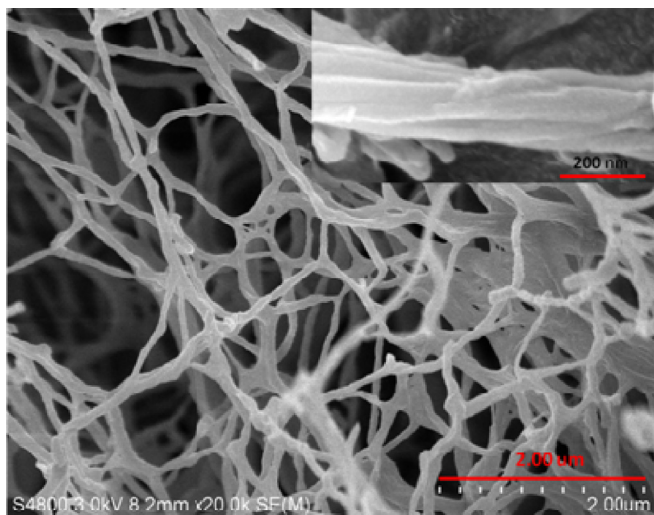


Fig. 1. SEM image of xerogel prepared from cyclohexane solution for **T2**.

tens of micrometers in length, which further cross-link to form a 3-D network. These fibers formed right-handed helices (Inset in Fig. 1), which was in accordance with the CD spectroscopy (Fig. S1).

3.3. Gelation-induced fluorescence-enhanced emission

To investigate the interrelationship between the emission and aggregation modes along with the sol–gel transition, temperature-dependent fluorescence spectra of **T2** with a high concentration in the cyclohexane (20 mg/mL) were measured from 70 to 25 °C. As shown in Fig. 2, the initial solution of **T2** exhibited rather weak fluorescence. And the fluorescence intensity increased along with the decrease in temperature. The remarkable fluorescence enhancement from the gels was possibly due to the formation of self-assembly aggregates [30,40]. Interestingly, the fluorescence intensity of **T2** can be reversibly modulated accompanying the gel–sol transition through alternating cooling and heating (Inset of Fig. 2). Furthermore, the obvious enhancement of fluorescence intensity after gelating could easily be distinguished even by naked eyes from the photographic images (Inset of Fig. 2). The remarkable

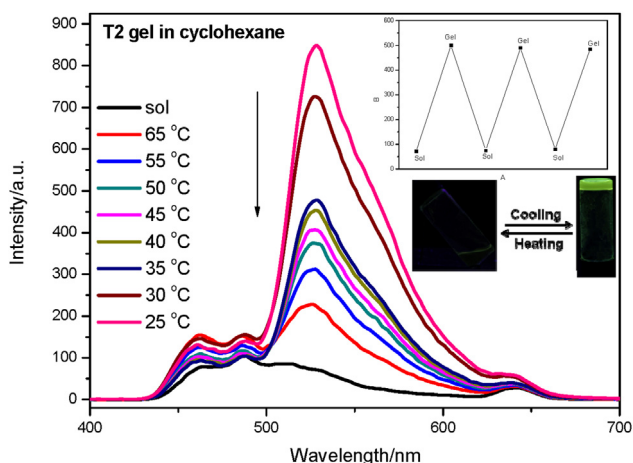


Fig. 2. Temperature-dependent fluorescence spectra of **T2** in cyclohexane (20 mg/mL, $\lambda_{\text{ex}} = 324$ nm). Insets show the reversible variation of the emission intensity at 528 nm accompanying the sol–gel transition (top) and the emission images of the **T2** in sol (left) and gel (right) state under UV irradiation at 365 nm (bottom).

fluorescence enhancement from gels was belonged to gelation-induced fluorescence enhanced emission [41].

3.4. AIE properties

The UV–Vis absorption and PL emission behaviors of the diluted mixtures of the compounds were studied in a mixture of water-THF with different water fractions to determine their AIE properties. The PL spectra of **T1** and **T2** in THF/water mixtures with different water contents are shown in Fig. 3. For **T1**, the PL intensity was very weak in pure THF and in the mixtures with water fraction <30%, and then the PL intensity increased with the increase in water fraction. When the water fraction reached 90%, a dramatic enhancement in luminescence was observed. However, there were some differences of **T2** with the increase in water fraction. When the water fraction reached 60% and 70%, it could easily form floccus aggregation with the PL intensity stronger than the water fraction of 90%. This phenomenon was often observed in some compounds with AIE properties, but the reasons remain unclear. There are two possible explanations for this phenomenon: (1) after the aggregation, only the molecules on the surface of the nanoparticles emitted light and contributed to the fluorescent intensity upon excitation, leading to a decrease in fluorescent intensity. However, the restriction of intramolecular rotations of the aromatic rings around the carbon–carbon single bonds in the aggregation state could enhance light emission. The net outcome of these antagonistic processes depends on which process plays a predominant role in affecting the fluorescent behavior of the aggregated molecules; (2) when water is added, the solute molecules can aggregate into two kinds of nanoparticle suspensions: crystal particles and amorphous particles. The former leads to an enhancement in the PL intensity, while the latter leads to a reduction in intensity. Thus, the measured overall PL intensity data depends on the combined actions of the two kinds of nanoparticles [42–48]. Careful inspection of the PL spectra of the dye in the aqueous mixtures reveals a slight red shift (~3 nm) in the emission peak when the water fraction is increased from 60% to 90%. This phenomenon often observed in some compounds with AIEE properties and has been observed and theorized by Tang et al. This is probably due to the change in the packing mode of the dye molecules in the aggregates. In the mixture with the “low” water fraction, solute molecules steadily assemble in an ordered pattern to form more emissive, bluer crystalline aggregates. In a mixture with “high” water content, solute molecules quickly agglomerate in a random way to form less emissive, redder amorphous particles [42,43]. This result indicated that both compounds exhibited obvious AIE activity. The AIE activity may be attributed to its twisted structure (Fig. 4), in which multiple phenyl peripheries linked to an ethylene core via C_{phenyl}–C_{ethenyl} single bonds which enable their free rotation. The molecular size and effect of steric hindrance influence their rotation; a larger molecule should have lower freedom of rotation [7,49].

The UV/vis absorption spectra of **T1** and **T2** in the THF/water mixtures (2.5 mM) were provided in the Supporting Information, Fig. S2. The spectra displayed absorption tails extending well into the long wavelength region caused by the Mie effect [38,49–51], indicating that the molecules aggregated into nanoparticles in the mixtures. The different SEM images of **T2** obtained from the mixed solutions containing 0%, 50%, 60%, 70%, 80% and 90% volume fractions of water shown in Fig. 5. The result shows that **T2** forms particles of a few hundred nanometers in size in water fractions of 50%, 80%, 90%, while it forms fibers about a few hundred nanometers in width in the water fraction of 60% and 70%.

Quantum mechanical computations were conducted using the Materials Studio 7.0 software to study the lowest energy spatial conformation of the compounds [52]. The highest occupied

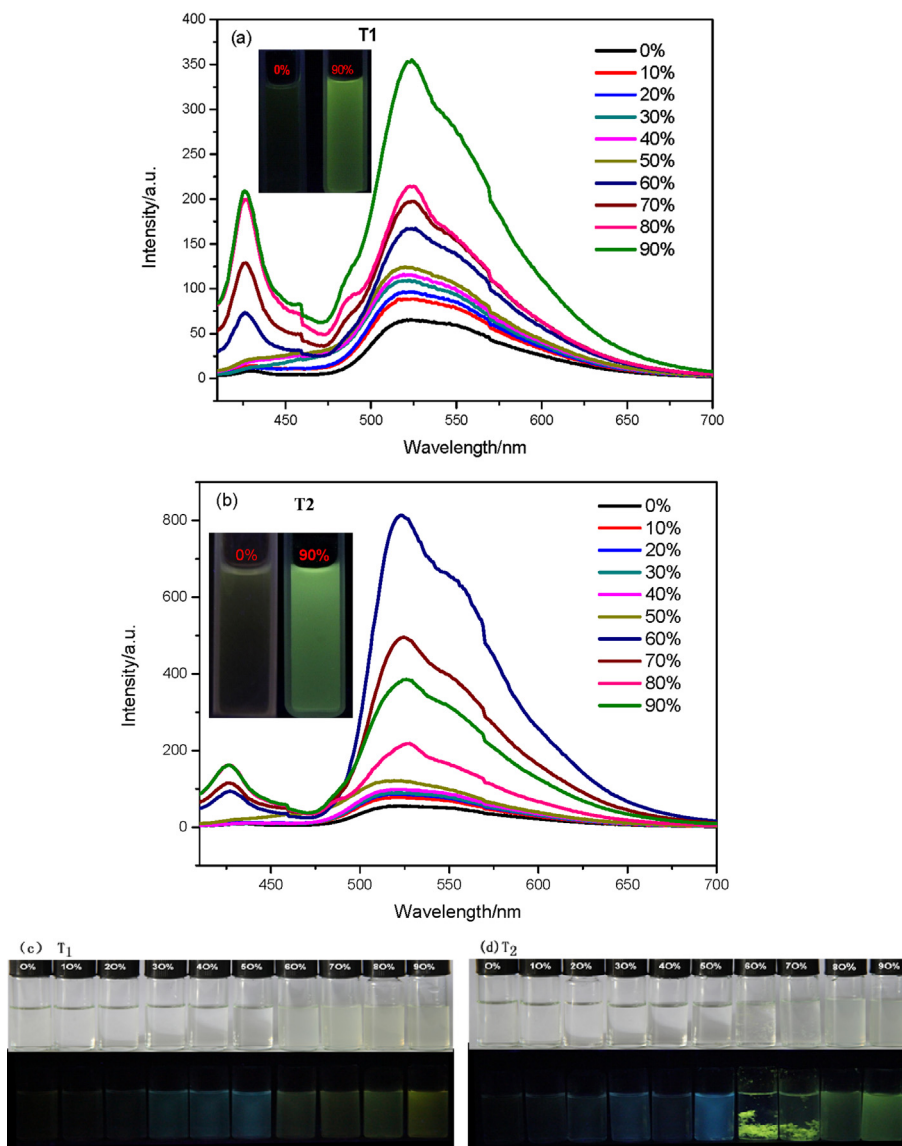


Fig. 3. PL spectra of **T1** (a) and **T2** (b) in THF/water mixtures with different water fractions (Inset: the images were taken at room temperature under 365 nm UV light in THF and 90% water), concentration 2.5 mM, $\lambda_{\text{ex}} = 321$ nm for **T1** and $\lambda_{\text{ex}} = 324$ nm for **T2**; the images of **T1** (c) and **T2** (d) in THF/water mixtures with different water fractions were taken under room light (top) and 365 nm UV light (bottom).

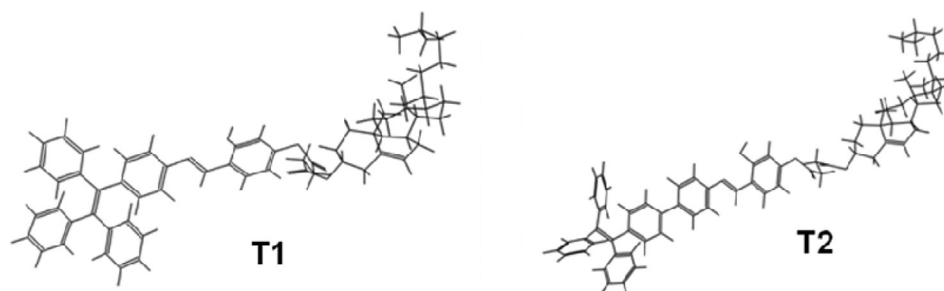


Fig. 4. The optimized structures of the compounds.

molecular orbitals (HOMOs) and the lowest unoccupied molecular orbitals (LUMOs) of these compounds were obtained (Fig. 6) after structural optimization. **T1** and **T2** showed different electron cloud distributions in either their HOMO or LUMO orbital, which illustrates why **T1** and **T2** exhibited very different UV and PL spectra. As

shown in Fig. 6, the electron cloud distributions in HOMO of **T1** was mainly localized at the tetraphenylethylene and the salicylaldehyde moieties, while **T2** was localized at the tetraphenylethylene core. Meanwhile, the electron cloud distributions in HOMO of **T2** were more disperse than **T1**, respectively. Moreover, the energy gap

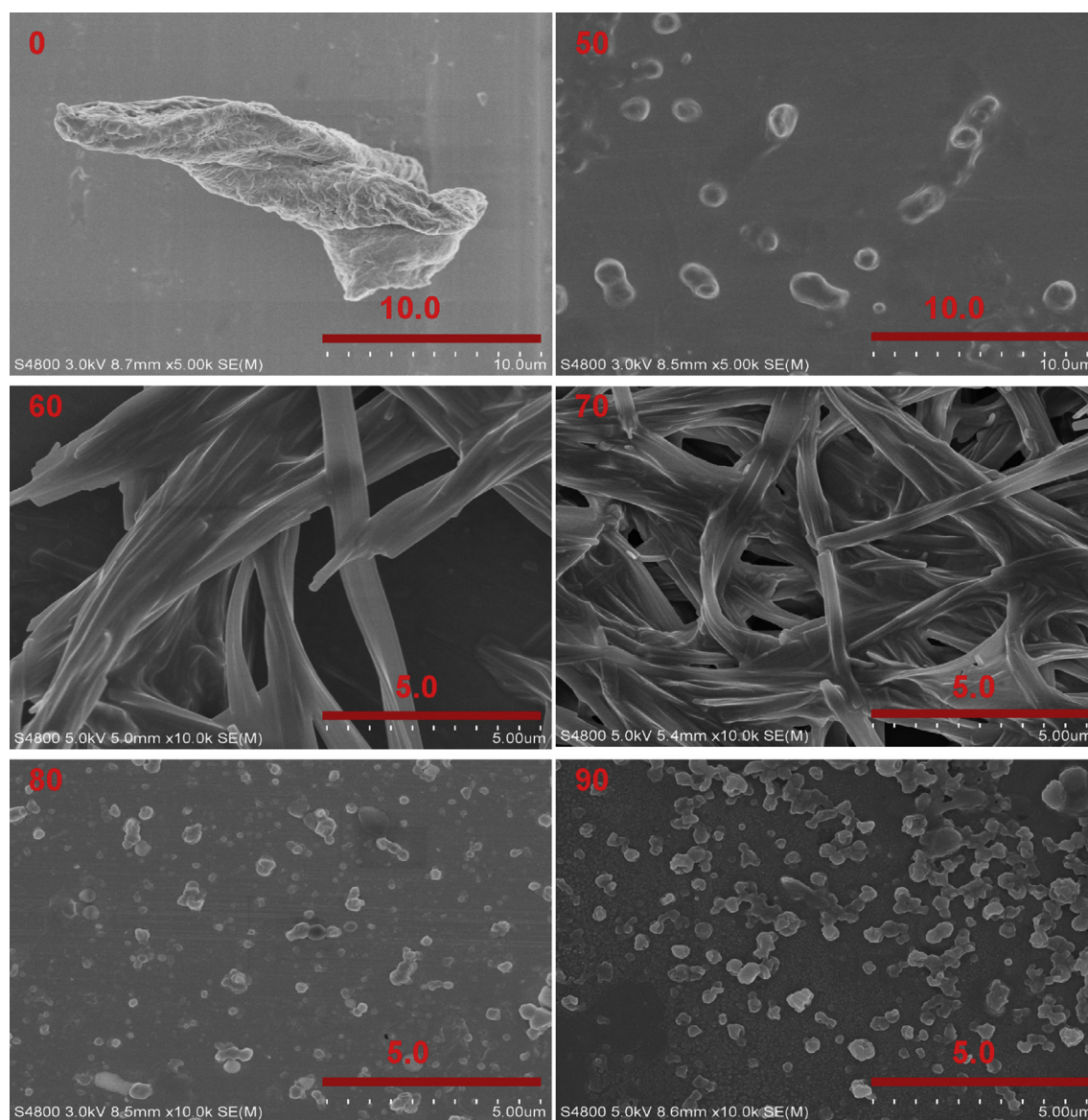


Fig. 5. SEM images of water/THF (v/v) mixture of T2.

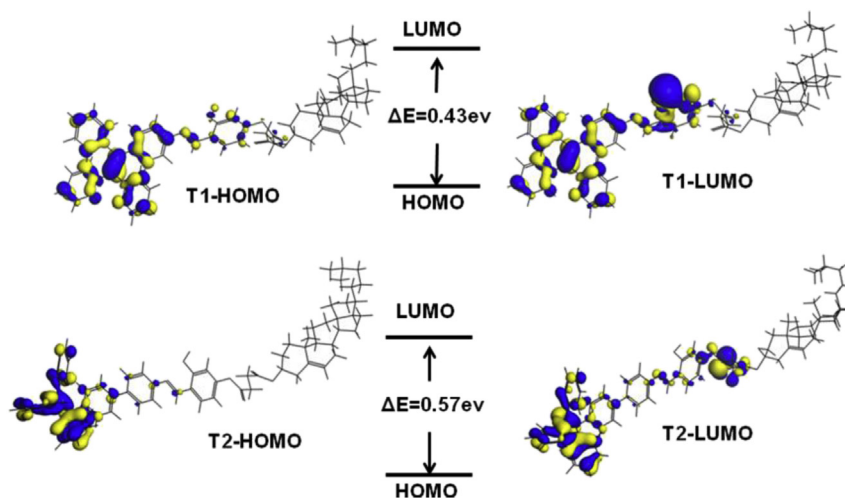


Fig. 6. Molecular orbital amplitude plots of HOMO and LUMO energy levels of T1 and T2.

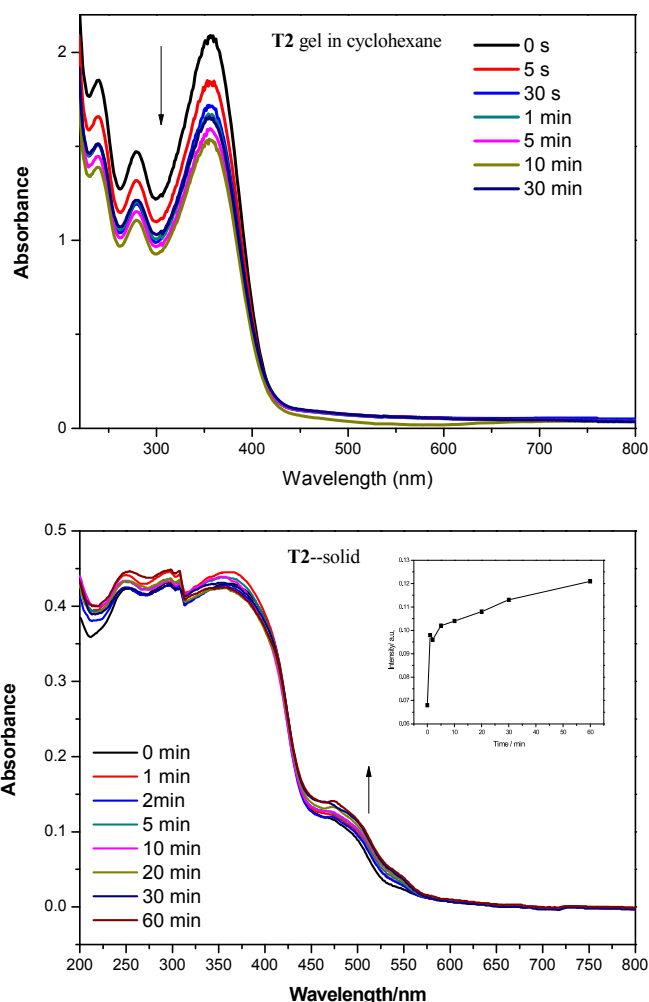


Fig. 7. UV–Vis spectra of **T2** in cyclohexane gel (a) and in solid state (b) by prolonged irradiation under 365 nm light from a high-pressure mercury lamp. Inset: the plot of the absorbance at 500 nm as a function of the irradiation time.

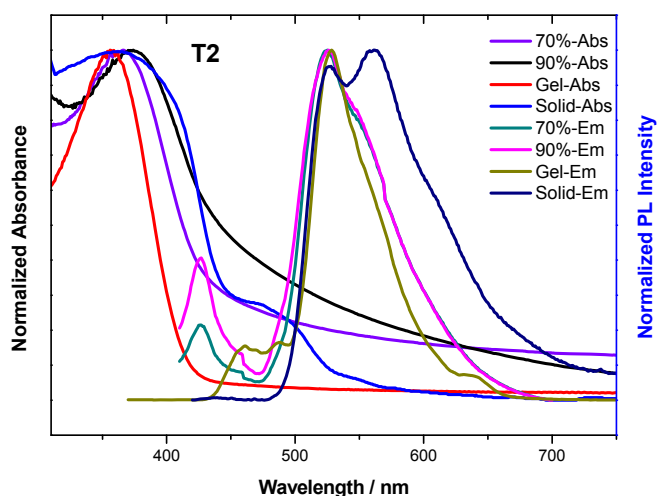


Fig. 8. Absorption and emission spectra of **T2** under different conditions.

between the HOMO and LUMO of **T2** (0.57 eV) is larger than **T1** (0.43 eV), which may explain the following photochromism behavior of these compounds.

Table 2
The absorption and emission peaks of **T1** and **T2**.

Sample	State	λ_{abs} (nm)	λ_{E^*} (nm)	λ_{K^*} (nm)	Stoke shift (nm)
T1	90%	368	426	524	156
	Solid	340	–	565	225
T2	70%	364	427	525	161
	90%	375	427	526	151
	Gel	356	462	528	172
	Solid	360	–	527,561	201

3.5. Photochromic properties

The salicylideneaniline crystals usually exhibit two mutually exclusive properties: either thermochromism or photochromism [3,53–59]. The UV absorption spectra of the compounds **T1** and **T2** were measured at three different states (i.e., solution, gel and solid) with variable irradiation time under 365 nm light (Fig. 7 and Fig. S3). After irradiation with 365 nm light, **T2** in the solutions of DMF and THF stayed almost unchanged at 280 nm and 358 nm (Fig. S3). However, the band at 280 nm and 358 nm of **T2** in cyclohexane gel showed decrease under the prolonged irradiation, and a new peak of **T2** in solid powder appeared at 425 nm–575 nm intensified along with the prolonged irradiation. **T1** only showed very slight change from 425 nm to 525 nm (Fig. S3). This spectrum suggests that **T2** shows significant photochromic properties in both the gel and the solid phase [3]. It is attributed that the TPE moiety possessing a twisted spatial conformation, which makes the molecular packing relatively loose. Moreover, **T2** has one more phenyl ring than **T1** among the link of TPE and *o*-hydroxyl benzene ring to make the molecular packing much looser than **T1**, so the *cis*-*trans* keto isomerization of the photo-product is possible due to the very loose packing. Thus **T2** exhibits the property of photochromism [52–58].

3.6. ESIPT process

Usually, an *o*-hydroxyl group on the benzene ring of schiff base was introduced to form an intramolecular hydrogen bond, which was responsible for ESIPT process and necessary for their AIE property at high concentrations or in the aggregate state due to their large Stokes shift [25–28]. To further verify the mechanism of ESIPT process, absorption and emission spectra of **T2** under different conditions were measured (Fig. 8, Table 2). Both **T1** and **T2** exhibited typical ESIPT behavior with a π - π^* transition peak at 356–375 nm in the absorption spectrum and dual bands in the emission spectrum, which comprised a weak E^* emission at 426–462 nm and a large Stokes' shifted (>150 nm) K^* emission at 525–565 nm, respectively. The detailed photoinduced isomerization and photoluminescence processes are shown in Fig. 9. **T2** has one phenyl ring more than **T1** between the link of TPE and *o*-hydroxyl benzene ring to make the molecular packing much looser than **T1**. **T1** might undergo a transition from the excited state to the ground state accompanied by a longer emission wavelength, and then return to the *E*-OH ground state rapidly with a large Stokes shift (225 nm) but no photochromism. For **T2**, there is enough space to permit the molecular to rotate, thus make the *Z*-NH form transform into the *E*-NH form possible exhibiting photochromism. These results were in agreement with the time-resolved emission-decay spectra.

The time-resolved emission-decay behavior of these compounds under different conditions was also studied. The time-resolved fluorescence curves and the lifetime data are illustrated in Fig. 10 and Table 3. In all cases, the emission can fit the double exponential decay. The lifetimes may be correlated to the various

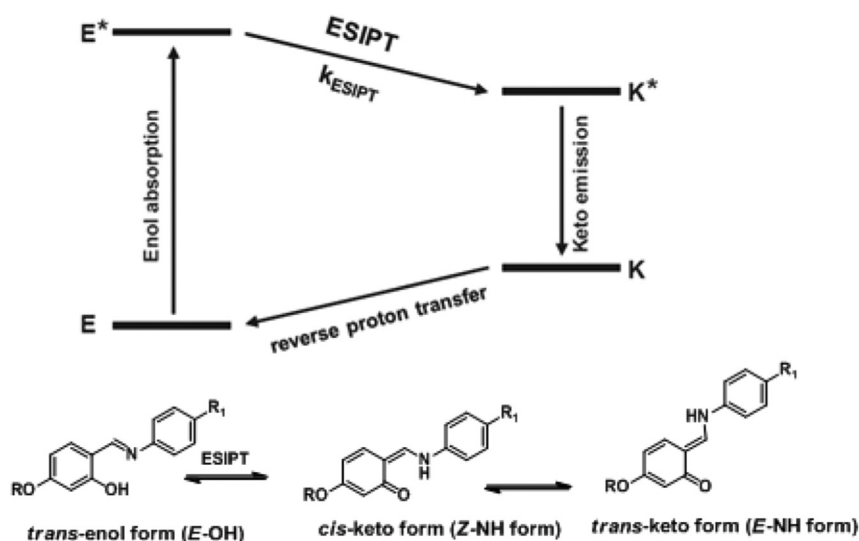


Fig. 9. Photoinduced isomerization and photoluminescence processes of a typical salicylideneaniline moiety.

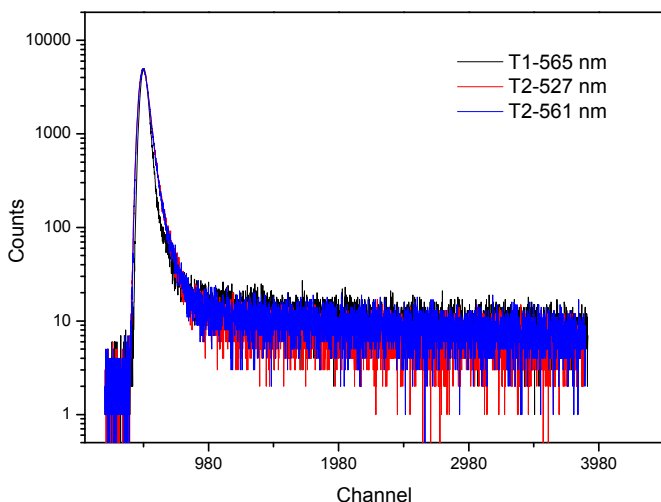
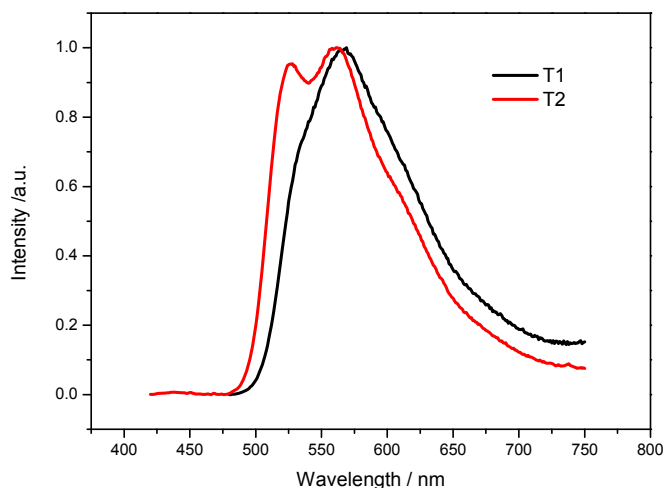


Fig. 10. (a) Fluorescence spectra (λ_{ex} : 380 nm) and (b) Fluorescence decay (λ_{em} : T1 (565 nm), T2 (527 nm and 561 nm)) of the compounds T1 and T2 in the solid state at 25 °C.

Table 3

Solid-state fluorescence lifetime data of T1 and T2 samples under different conditions.

Sample	λ_{em}	τ_1 (ns) ^a	τ_2 (ns) ^a	A_1 ^b	A_2 ^b	$\langle \tau \rangle$ (ns) ^c
T1	565	0.35	1.80	85.00	15.00	0.57
T2	527	1.05	3.72	92.00	8.00	1.26
	561	1.05	3.72	92.00	8.00	1.26

^a Fluorescence lifetime.

^b Fractional contribution.

^c Weighted mean lifetime.

ground state aggregates, excimers and charge-transfer dimer emissions [7,60]. The weighted mean lifetime $\langle \tau \rangle$ of T2 (1.26 ns) was much longer than T1 (0.57 ns), which are in good agreement with its optical energy gap, suggesting that energy transfer of T1 in the excited state provided by the proton transfer across the OH ... N hydrogen bond is faster than T2.

4. Conclusion

In summary, two novel AIE compounds, T1 and T2 based on salicylideneaniline harnessing ES IPT process have been designed and synthesized. T2 could form gel in cyclohexane, exhibiting gelation-induced enhanced emission behavior attributed to the formation of self-assembly aggregates. Their fluorescence intensities could be reversibly changed with gel–sol transition by alternatively cooling and heating. SEM images and CD spectra revealed that the gelator molecule self-assembled into 1D helical fiber with diameters of approximately 100 nm and further twisted into 3D networks. Meanwhile, T2 shows significant photochromic properties in both the gel and the solid phase under UV irradiation due to the loose packing of the molecules and permitting the molecule to rotate, thus indicating that it may be a potential candidate for external stimuli-responsive materials through tuning the self-assembly process of the functional gelator.

Acknowledgments

This work was financially supported by NSFC (21372194, 21476075 and 21272072) and the Guangdong Yangfan Talent Plan (2013). M. Luo and C. Li also acknowledge the Research Funds of

Lingnan Normal University (QL1515 & QL1402).

Appendix A. Supplementary data

Supplementary data related to this article can be found at <http://dx.doi.org/10.1016/j.dyepig.2016.04.036>.

References

- [1] Babu SS, Praveen VK, Ajayaghosh A. Functional π -gelators and their applications. *Chem Rev* 2014;114(4):1973–2129.
- [2] Meazza L, Foster JA, Fucke K, Metrangolo P, Resnati G, Steed JW. Halogen-bonding-triggered supramolecular gel formation. *Nat Chem* 2013;5(1):42–7.
- [3] Xue P, Lu R, Lu R, Zhang Y, Nomoto H, Takafuji M, et al. Functional organogel based on a salicylideneaniline derivative with enhanced fluorescence emission and photochromism. *Chem Eur J* 2007;13(29):8231–9.
- [4] Wang S, Shen W, Feng Y, Tian H. A multiple switching bisthiénylene and its photochromic fluorescent organogelator. *Chem Commun* 2006;(14):1497–9.
- [5] Zhang M, Xu D, Yan X, Chen J, Dong S, Zheng B, et al. Self-healing supramolecular gels formed by crown ether based host-guest interactions. *Angew Chem Int Ed* 2012;51(28):7011–5.
- [6] Chen Q, Zhang D, Zhang G, Yang X, Feng Y, Fan Q, et al. Multicolor tunable emission from organogels containing tetraphenylethene, peryleneimide, and spiropyran derivatives. *Adv Funct Mater* 2010;20(19):3244–51.
- [7] Luo M, Zhou X, Chi Z, Liu S, Zhang Y, Xu J. Fluorescence-enhanced organogelators with mesomorphic and piezofluorochromic properties based on tetraphenylethylene and gallic acid derivatives. *Dyes Pigments* 2014;101:74–84.
- [8] Jung JH, Kobayashi H, Masuda M, Shimizu T, Shinkai S. Helical ribbon aggregate composed of a crown-appended cholesterol derivative which acts as an amphiphilic gelator of organic solvents and as a template for chiral silica transcription. *J Am Chem Soc* 2001;123:8785–9.
- [9] Jung JH, Kobayashi H, van Bommel KJ, Shinkai S, Shimizu T. Creation of novel helical ribbon and double-layered nanotube TiO₂ structures using an organogel template. *Chem Mater* 2002;14:1445–7.
- [10] Yang X, Zhang G, Zhang D. Stimuli responsive gels based on low molecular weight gelators. *J Mater Chem* 2012;22(1):38–50.
- [11] Wu J, Yi T, Shu T, Yu M, Zhou Z, Xu M, et al. Ultrasound switch and thermal self-repair of morphology and surface wettability in a cholesterol-based self-assembly system. *Angew Chem Int Ed* 2008;120(6):1079–83.
- [12] Ma X, Wang Q, Qu D, Xu Y, Ji F, Tian H. A Light-driven pseudo[4]rotaxane encoded by induced circular dichroism in a hydrogel. *Adv Funct Mater* 2007;17(5):829–37.
- [13] Zhang Q, Qu DH, Ma X, Tian H. Sol-gel conversion based on photoswitching between noncovalently and covalently linked netlike supramolecular polymers. *Chem Commun* 2013;49(84):9800–2.
- [14] Kobayashi H, Friggeri A, Koumoto K, Amaike M, Shinkai S, Reinhoudt DN. Molecular design of “super” hydrogelators: understanding the gelation process of azobenzene-based sugar derivatives in water. *Org Lett* 2002;4(9):1423–6.
- [15] Li Y, Wong KM-C, Tam AY-Y, Wu L, Yam V-W. Thermo- and acid-responsive photochromic spironaphthoxazine-containing organogelators. *Chem Eur J* 2010;16(29):8690–8.
- [16] Zhang Q, Yao X, Qu DH, Ma X. Multistate self-assembled micro-morphology transitions controlled by host-guest interactions. *Chem Commun* 2014;50(13):1567–9.
- [17] Chung JW, An B-K, Park SYA. Thermoreversible and proton-induced gel-sol phase transition with remarkable fluorescence variation. *Chem Mater* 2008;20:6750–5.
- [18] Yan N, He G, Zhang H, Ding L, Fang Y. Glucose-based fluorescent low-molecular mass compounds: creation of simple and versatile supramolecular gelators. *Langmuir* 2010;26(8):5909–17.
- [19] Sun F, Zhang G, Zhang D. A new gelator based on tetraphenylethylene and diphenylalanine: gel formation and reversible fluorescence tuning. *Chin Sci Bull* 2012;57(33):4284–8.
- [20] Murata K, Aoki M, Suzuki T, Harada T, Kawabata K, Komori K, et al. Thermal and light control of the sol-gel phase transition in cholesterol-based organic gels. novel helical aggregation modes as detected by circular dichroism and electron microscopic observation. *J Am Chem Soc* 1994;116(15):6664–76.
- [21] Kwon JE, Park SY. Advanced organic optoelectronic materials: harnessing excited-state intramolecular proton transfer (ESIPT) process. *Adv Mater* 2011;23(32):3615–42.
- [22] Luo J, Xie Z, Lam JWY, Cheng L, Tang BZ, Chen H, et al. Aggregation-induced emission of 1-methyl-1,2,3,4,5-pentaphenyl-silole. *Chem Commun* 2001;18:1740–1.
- [23] Yuning H, Lam JWY, Tang BZ. Aggregation-induced emission. *Chem Soc Rev* 2011;40:5361–88.
- [24] Mei J, Leung NLC, Kwok RTK, Lam JWY, Tang BZ. Aggregation-induced emission: together we shine, united we soar! *Chem Rev* 2015;115(21):11718–940.
- [25] Liu H, Wei R, Xiang Y, Tong A. Fluorescence turn-on detection of pyrophosphate based on aggregation-induced emission property of 5-chlorosalicylaldehyde azine. *Anal Methods* 2015;7(2):753–8.
- [26] Liu H, Wang X, Xiang Y, Tong A. Fluorescence turn-on detection of cysteine over homocysteine and glutathione based on “ESIPT” and “AIE”. *Anal Methods* 2015;7(12):5028–33.
- [27] Peng L, Gao M, Cai X, Zhang R, Li K, Feng G, et al. A fluorescent light-up probe based on AIE and ESIPT processes for β -galactosidase activity detection and visualization in living cells. *J Mater Chem B* 2015;3(47):9168–72.
- [28] Fihey A, Perrier A, Browne WR, Jacquemin D. Multiphotochromic molecular systems. *Chem Soc Rev* 2015;44(11):3719–59.
- [29] Nayak MK, Kim B-H, Kwon JE, Park S, Seo J, Chung JW, et al. Gelation-induced enhanced fluorescence emission from organogels of salicylanilide-containing compounds exhibiting excited-state intramolecular proton transfer: synthesis and self-assembly. *Chem Eur J* 2010;16(25):7437–47.
- [30] Chen P, Lu R, Xue P, Xu T, Chen G, Zhao Y. Emission enhancement and chromism in a salen-based gel system. *Langmuir* 2009;25(15):8395–9.
- [31] Ren YY, Wu NW, Huang J, Xu Z, Sun DD, Wang CH, et al. A neutral branched platinum-acetylacetonate complex possessing a tetraphenylethylene core: preparation of a luminescent organometallic gelator and its unexpected spectroscopic behavior during sol-to-gel transition. *Chem Commun* 2015;51(82):15153–6.
- [32] Zhang C, Li Y, Xue X, Chu P, Liu C, Yang K, et al. A smart pH-switchable luminescent hydrogel. *Chem Commun* 2015;51(20):4168–71.
- [33] Qin A, Tang B. Aggregation-induced emission: applications. Wiley; 2013. p. 1–275.
- [34] Liu B, Wang Z, Wu N, Li M, You J, Lan J. Discovery of a full-color-tunable fluorescent core framework through direct C-H (hetero)arylation of N-heterocycles. *Chem Eur J* 2012;18(6):1599–603.
- [35] Liu G, Wu D, Liang J, Han X, Liu SH, Yin J. Tetraphenylethene modified [n] rotaxanes: synthesis, characterization and aggregation-induced emission behavior. *Org Biomol Chem* 2015;13(13):4090–100.
- [36] Han X, Cao M, Xu Z, Wu D, Chen Z, Wu A, et al. Aggregation-induced emission behavior of a pH-controlled molecular shuttle based on a tetraphenylethene moiety. *Org Biomol Chem* 2015;13(38):9767–74.
- [37] Dou C, Chen D, Iqbal J, Yuan Y, Zhang H, Wang Y. Multistimuli-responsive benzothiadiazole-cored phenylene vinylene derivative with nanoassembly properties. *Langmuir* 2011;27(10):6323–9.
- [38] Seo SH, Tew GN, Chang JY. Lyotropic columnar liquid crystals based on polycatenar 1H-imidazole amphiphiles and their assembly into bundles at the surface of silicon. *Soft Matter* 2006;2(10):886.
- [39] Yao X, Wang X, Jiang T, Ma X, Tian H. Bis-p-sulfonatocalix[4]arene-based supramolecular amphiphiles with an emergent lower critical solution temperature behavior in aqueous solution and hydrogel. *Langmuir* 2015;31(51):13647–54.
- [40] Abraham S, Vijayaraghavan RK, Das S. Tuning microstructures in organogels: gelation and spectroscopic properties of mono- and bis-cholesterol-linked diphenylbutadiene derivatives. *Langmuir* 2009;25(15):8507–13.
- [41] Zhu L, Ma X, Ji F, Wang Q, Tian H. Effective enhancement of fluorescence signals in rotaxane-doped reversible hydrogel systems. *Chemistry* 2007;13(33):9216–22.
- [42] Li H, Chi Z, Zhang X, Xu B, Liu S, Zhang Y, et al. New thermally stable aggregation-induced emission enhancement compounds for non-doped red organic light-emitting diodes. *Chem Commun* 2011;47(40):11273–5.
- [43] Dong Y, Lam JW, Qin A, Sun J, Liu J, Li Z, et al. Aggregation-induced and crystallization-enhanced emissions of 1,2-diphenyl-3,4-bis(diphenylmethylene)-1-cyclobutene. *Chem Commun* 2007;(31):3255–7.
- [44] Zhang X, Yang Z, Chi Z, Chen M, Xu B, Wang C, et al. A multi-sensing fluorescent compound derived from cyanoacrylic acid. *J Mater Chem* 2010;20(2):292–8.
- [45] Xu BJ, Chi ZG, Li XF, Li HY, Zhou W, Zhang XQ, et al. Synthesis and properties of diphenylcarbazole triphenylethylene derivatives with aggregation-induced emission, blue light emission and high thermal stability. *J Fluoresc* 2011;21(1):433–41.
- [46] Xu B, Chi Z, Yang Z, Chen J, Deng S, Li H, et al. Facile synthesis of a new class of aggregation-induced emission materials derived from triphenylethylene. *J Mater Chem* 2010;20(20):4135.
- [47] Li H, Chi Z, Xu B, Zhang X, Yang Z, Li X, et al. New aggregation-induced emission enhancement materials combined triarylamine and dicarbazoyl triphenylethylene moieties. *J Mater Chem* 2010;20(29):6103.
- [48] Xu B, Chi Z, Li H, Zhang X, Li X, Liu S, et al. Synthesis and properties of aggregation-induced emission compounds containing triphenylethene and tetraphenylethene moieties. *J Phys Chem C* 2011;115(35):17574–81.
- [49] Zhang X, Chi Z, Xu B, Li H, Yang Z, Li X, et al. Synthesis of blue light emitting bis(triphenylethylene) derivatives: a case of aggregation-induced emission enhancement. *Dyes Pigments* 2011;89(1):56–62.
- [50] Xu B, Chi Z, Zhang J, Zhang X, Li H, Li X, et al. Piezofluorochromic and aggregation-induced-emission compounds containing triphenylethylene and tetraphenylethylene moieties. *Chem Asian J* 2011;6(6):1470–8.
- [51] Zhang X, Chi Z, Li H, Xu B, Li X, Liu S, et al. Synthesis and properties of novel aggregation-induced emission compounds with combined tetraphenylethylene and dicarbazoyl triphenylethylene moieties. *J Mater Chem* 2011;21(6):1788–96.
- [52] He Zikai, Shan Liang, Mei Ju, Wang Hong, Lam Jacky WY, Sung Herman HY, et al. Aggregation-induced emission and aggregation-promoted photochromism of bis(diphenylmethylene)dihydroacenes. *Chem Sci* 2015;6:3538–43.
- [53] Hadjoudis E, Mavridis IM. Photochromism and thermochromism of Schiff bases in the solid state: structural aspects. *Chem Soc Rev* 2004;33(9):579–88.

- [54] Tian H, Yang S. Recent progresses on diarylethene based photochromic switches. *Chem Soc Rev* 2004;33(2):85–97.
- [55] Tian H, Wang S. Photochromic bisthiénylene as multi-function switches. *Chem Commun* 2007;(8):781–92.
- [56] Yao X, Li T, Wang S, Ma X, Tian H. A photochromic supramolecular polymer based on bis-p-sulfonatocalix[4]arene recognition in aqueous solution. *Chem Commun* 2014;50(54):7166–8.
- [57] Hu F, Cao M, Ma X, Liu SH, Yin J. Visible-light-dependent photocyclization: design, synthesis, and properties of a cyanine-based dithienylene. *J Org Chem* 2015;80(15):7830–5.
- [58] Yao X, Ma X, Tian H. Aggregation-induced emission encoding supramolecular polymers based on controllable sulfonatocalixarene recognition in aqueous solution. *J Mater Chem C* 2014;2(26):5155.
- [59] Kundu PK, Samanta D, Leizrowice R, Margulis B, Zhao H, Borner M, et al. Light-controlled self-assembly of non-photoresponsive nanoparticles. *Nat Chem* 2015;7(8):646–52.
- [60] Zhang G, Singer JP, Kooi SE, Evans RE, Thomas EL, Fraser CL. Reversible solid-state mechanochromic fluorescence from a boron lipid dye. *J Mater Chem* 2011;21(23):8295.